A new white dwarf companion around the $\Delta\mu$ star GJ 3346

M. Bonavita [1,2]★, C. Fontanive [3], S. Desidera,[4] V. D'Orazi,[4] A. Zurlo,[5,6] K. Mužić [7], B. Biller, [1,2] R. Gratton,[4] D. Mesa[4] and A. Sozzetti[8]

[1]*SUPA, Institute for Astronomy, University of Edinburgh, Blackford Hill, Edinburgh EH9 3HJ, UK*
[2]*Centre for Exoplanet Science, University of Edinburgh, Edinburgh EH9 3HJ, UK*
[3]*Center for Space and Habitability, University of Bern, Gesellschaftsstrasse 6, CH-3012 Bern, Switzerland*
[4]*INAF – Osservatorio Astronomico di Padova, Vicolo dell'Osservatorio 5, I-35121 Padova, Italy*
[5]*Núcleo de Astronomía, Facultad de Ingeniería y Ciencias, Universidad Diego Portales, Av. Ejercito 441 ,8370191 Santiago, Chile*
[6]*Escuela de Ingeniería Industrial, Facultad de Ingeniería y Ciencias, Universidad Diego Portales, Av. Ejercito 441, 8370191 Santiago, Chile*
[7]*CENTRA, Faculdade de Ciências, Universidade de Lisboa, Ed. C8, Campo Grande, P-1749-016 Lisboa, Portugal*
[8]*INAF – Osservatorio Astrofisico di Torino, Via Osservatorio 20, I-10025 Pino Torinese, Italy*

ABSTRACT

We present the discovery of a white dwarf companion at ∼3.6 arcsec from GJ 3346, a nearby ($\pi \sim 42$ mas) K star observed with SPHERE@VLT as part of an open time survey for faint companions to objects with significant proper motion discrepancies ($\Delta\mu$) between *Gaia* DR1 and Tycho-2. Syrius-like systems like GJ 3346 AB, which include a main-sequence star and a white dwarf, can be difficult to detect because of the intrinsic faintness of the latter. They have, however, been found to be common contaminants for direct imaging (DI) searches. White dwarfs have in fact similar brightness to substellar companions in the infrared, while being much brighter in the visible bands like those used by *Gaia*. Combining our observations with *Gaia* DR2 and with several additional archival data sets, we were able to fully constrain the physical properties of GJ 3346 B, such as its effective temperature ($11 \times 10^3 \pm 500$ K) as well as the cooling age of the system (648 ± 58 Myr). This allowed us to better understand the system history and to partially explain the discrepancies previously noted in the age indicators for this object. Although further investigation is still needed, it seems that GJ 3346, which was previously classified as young, is in fact most likely to be older than 4 Gyr. Finally, given that the mass (0.58 ± 0.01 $M_\odot$) and separation (85 au) of GJ 3346 B are compatible with the observed $\Delta\mu$, this discovery represents a further confirmation of the potential of this kind of dynamical signatures as selection methods for DI surveys targeting faint, substellar companions.

Key words: instrumentation: adaptive optics – binaries: visual – white dwarfs.

1 INTRODUCTION

Long-term proper motion measurements provided by historical catalogues like Tycho-2 (Høg et al. 2000) can be a good approximation of the motion of the centre of mass of binaries with sufficiently long periods. Short-term measurements such as the ones provided by the *Hipparcos* (Perryman et al. 1997) or, more recently, by the European Space Agency (ESA) cornerstone mission *Gaia* (Gaia Collaboration 2016a), can instead capture the reflex orbital motion of the pair. A significant difference ($\Delta\mu$) between proper motion measurements can therefore be interpreted as a good indication of the presence of a perturbing body around a seemingly single star. Targeted searches for companions compatible with measured trends

between the *Hipparcos* and Tycho-2 catalogues (see e.g. Makarov & Kaplan 2005) have been highly successful (see e.g. Tokovinin et al. 2012; Tokovinin, Hartung & Hayward 2013), confirming the power of such selection method.

The discovery space of these searches is of course limited by the precision of the available measurements, which explains why previous surveys were only able to target stellar-like companions. The first two intermediate *Gaia* data releases (*Gaia* DR1 and GR2; Gaia Collaboration 2016b, 2018) already allow the community to access the processed and calibrated data collected by the spacecraft in its first 22 months of operation. The five-parameter astrometric solution based on *Gaia* data only is now available for more than 1.3 billion sources, including proper motion measurements with uncertainties below 0.06 mas yr^{-1} for the brightest sources. As recently demonstrated by Fontanive et al. (2019b) with the new COPAINS (Code for Orbital Parametrization of Astrometrically

★ E-mail: mbonav@roe.ac.uk

Inferred New Systems) tool and previously by Brandt (2018), such an exquisite precision allows to unveil much smaller trends, effectively extending the $\Delta\mu$ searches below the substellar mass limit.

Astrometric signatures could therefore represent a powerful tool to maximize the number of direct detections of wide substellar companions. As these objects seem to be rare (see e.g. Vigan et al. 2017), a carefully pre-selected sample may in fact lead to a higher number of detections, compared to a blind search. In addition to precise astrometry, *Gaia* DR2 also provides multiband photometry for a considerable amount of sources, allowing to better characterize the faint companions detected via direct imaging (DI). *Gaia* colours hence make it possible to identify contaminants such as the so-called Sirius-like systems, composed by a main-sequence star of spectral type earlier than M and a white dwarf (hereafter WD) companion (Holberg et al. 2013). The faint WD would appear very similar to a young planetary or brown dwarf companion in the infrared, while being much brighter in the visible bands surveyed by *Gaia*.

Because of the intrinsic faintness and small projected separation of the companions, the current census of Sirius-like systems is highly incomplete, even within a short distance from the Sun (few tens of pc). The use of state-of-the-art high-contrast instrumentation has led to a number of discoveries in the last few years (Crepp et al. 2013, 2018; Zurlo et al. 2013), contributing towards reducing such incompleteness, and confirming the existence of an unseen population of WD companions in the close vicinity of the Sun, as predicted by Holberg et al. (2013).

The newly detected companions are typically found at rather small angular separations, corresponding to physical separations of few tens of au, and therefore close enough to have harboured some accretion phenomena. This makes them very useful benchmark objects to constrain wind accretion occurring in moderately wide binaries during the asymptotic giant branch (AGB) phase of the WD progenitor. They can also be used to investigate the maximum binary separation at which Ba-stars can be observed, as well as to characterize the rate of companion loss as a function of orbital periods.

Long-term radial velocity trends are observed in some cases, providing crucial clues towards the determination of dynamical masses. This, together with the availability of precise parallax measurements of the host star allows for a calibration of the progenitor mass (see e.g. Weidemann 2000) and the empirical mass radius relations (see e.g. Tremblay et al. 2017), as well as the luminosity function of WDs (see e.g. Holberg et al. 2016), although cases of discrepancy between the WD cooling age and properties of the companion have been previously reported (see e.g. Matthews et al. 2014).

Furthermore, some of the central stars show signatures of the impact of mass-loss from progenitors of WDs on the central stars. These include alterations of the rotation and therefore of the magnetic activity level (Desidera & Barbieri 2007; Zurlo et al. 2013, D'Orazi et al. in preparation), and alterations of chemical abundances of selected elements (Jeffries & Smalley 1996; Desidera, D'Orazi & Lugaro 2016), which could lead to a misclassification of the host as young star. These alterations may occur through direct mass exchange between the components (Roche lobe overflow, see e.g. McCrea 1964; Iben & Livio 1993) or, for wider binaries, by accretion of material lost during the AGB phase through stellar wind (wind accretion, see e.g. Jeffries & Stevens 1996; Boffin 2015). This latter mechanism appears to be relatively efficient in providing alterations even for binary separations of several tens of au. The occurrence of WD with moderately wide companions with chemical alterations of s-process elements and carbon (Jeffries & Smalley

1996) shows unambiguously that the origin of the accreted material is an AGB star (progenitor of the WD). Accretion of small amounts of material in these cases is also predicted by binary evolution codes (Hurley, Tout & Pols 2002). Furthermore, it should be considered the original separation of the binary system at the end of the AGB phase would have been smaller than the present one, because of the significant mass-loss experienced by the system (Hadjidemetriou 1963).

In this paper, we present the discovery of a WD companion to GJ 3346, one of the targets of the COPAINS pilot survey (Bonavita et. al, in preparation). The observational set-up and data reduction are described in Section 2. Section 3 presents the properties of the host star, and Section 4 presents the analysis of the properties of the new companion. Finally, our results are discussed and summarized in Section 5.

2 OBSERVATIONS AND DATA REDUCTION

GJ 3346 was observed as part of the COPAINS pilot survey (Bonavita et. al, in preparation), an open time SPHERE program (ID 100.C-0646) aimed at validating the COPAINS target selection process for DI systems, presented in Fontanive et al. (2019b). The goal of this study is to image unseen companions to stars selected with the COPAINS tool for their significant proper motion differences ($\Delta\mu$) between the astrometric values from the first *Gaia* data release and historical proper motions from the Tycho-2 catalogue. We note that the *Gaia* DR2 catalogue was not yet available at the time the survey was devised. Based on predictions from the COPAINS code (Fontanive et al. 2019b), the hidden companions responsible for the observed trends in the survey targets were expected to possibly be of substellar and in some cases of planetary nature (see Section 4.5).

In order to enhance our capability to detect such objects, despite their possible low luminosity, we therefore choose to use the SPHERE planet-finder instrument installed at the VLT (Beuzit et al. 2019), a highly specialized instrument, dedicated to high-contrast imaging and spectroscopy of young giant exoplanets. SPHERE is based on the SAXO extreme adaptive optics system (Fusco et al. 2006; Sauvage et al. 2010; Petit et al. 2014), which controls a deformable mirror with 41×41 actuators, and four control loops (fast visible tip-tilt, high-orders, near-infrared differential tip-tilt, and pupil stabilization). The common path optics employs several stress polished toric mirrors (Hugot et al. 2012) to transport the beam to the coronagraph and scientific instruments. Several types of coronagraphic devices for stellar diffraction suppression are provided, including apodized pupil Lyot coronagraphs (Soummer 2005) and achromatic four-quadrants phase masks (Boccaletti et al. 2008). The instrument has three science subsystems: the infrared dual-band imager and spectrograph (IRDIS; Dohlen et al. 2008), an integral field spectrograph (IFS; Claudi et al. 2008), and the Zimpol rapid-switching imaging polarimeter (ZIMPOL; Schmid et al. 2018).

The data were acquired on the 2018 January 29th (Table 1) in IRDIFS-EXT mode, using IRDIS in dual-band imaging (DBI; Vigan et al. 2010) mode with the $K_1 K_2$ filters ($\lambda_{K_1} = 2.1025 \pm 0.1020\,\mu m$; $\lambda_{K_2} = 2.2550 \pm 0.1090\,\mu m$), and IFS in the $Y - H$ ($0.97 - 1.66\,\mu m$, $R_\lambda = 30$) mode in pupil tracking. This combination enables the use of angular and/or spectral differential imaging techniques to improve the contrast performances at the subarcsecond level.

The observing sequence adopted was similar to those designed for the SHINE Guaranteed time survey (see e.g. Chauvin et al. 2017) and consisted of

Table 1. Details of VLT/SPHERE observations.

UT date	Instrument	Filter	Pl. scale (mas/pxl)	NDIT × DIT (s)	N_{exp}	Tot. FoV Rot. (°)	ω ($''$)	Strehl @ 1.6 μm	Airmass	TN (°)
29-01-2018	IRDIS	K1K2	12.250	1 × 64	17	17.5	0.58	0.85	1.39	−1.75
29-01-2018	IFS	Y-H	7.46	1 × 64	16					

(i) One point spread function (PSF) subsequence composed by a series of off-axis unsaturated images obtained with an offset of ∼0.4 arcsec relative to the coronagraph centre (produced by the tip-tilt mirror). A neutral density filter was used to avoid saturation[1] and the AO visible tip-tilt and high-order loops were closed to obtain a diffraction-limited PSF.

(ii) A *star centre* coronagraphic observation with four symmetric satellite spots, created by introducing a periodic modulation on the deformable mirror (see Langlois et al. 2012, for details), in order to enable an accurate determination of the star position behind the coronagraphic mask for the following deep coronagraphic sequence.

(iii) The deep coronagraphic subsequence, for which we used here the smallest apodized Lyot coronagraph (ALC-YH-S) with a focal-plane mask of 185 mas in diameter.

(iv) A new star centre sequence, a new PSF registration, as well as a short sky observing sequence for fine correction of the hot pixel variation during the night.

IRDIS and IFS data sets were reduced using the SPHERE Data Reduction and Handling (DRH) automated pipeline (Pavlov et al. 2008) at the SPHERE Data Center (SPHERE-DC, see Delorme et al. 2017) to correct for each data cube for bad pixels, dark current, flat-field and sky background. After combining all data cubes with an adequate calculation of the parallactic angle for each individual frame of the deep coronagraphic sequence, all frames are shifted at the position of the stellar centroid calculated from the initial star centre position. In order to calibrate the IRDIS and IFS data sets on sky, we used images of the astrometric reference field 47 Tuc observed with SPHERE at a date close to our observations. The plate scale and true north values used are reported in Table 1 and are based on the long-term analysis of the GTO astrometric calibration described by Maire et al. (2016).

The SPHERE-DC corrected products were then processed using the VIP (Vortex Image Processing Package) for high-contrast DI (Gomez Gonzalez et al. 2017), which allowed for the speckle pattern subtraction using the angular differential imaging (ADI: Marois et al. 2006) technique within a principal component analysis (PCA) algorithm (see Amara & Quanz 2012; Soummer, Pueyo & Larkin 2012 for details).

The resulting IRDIS K_1 combined image is shown in Fig. 1, with the position of the newly discovered companion highlighted by the white circle. Fig. 2 shows the corresponding 5σ contrast limit as a function of separation from the primary for both IRDIS filters. The bump at ∼3.6 arcsec is caused by the presence of the companion, which position is marked by the X signs.

3 HOST STAR PROPERTIES

As mentioned in Section 2, GJ 3346 was selected as target for our SPHERE program because of significant discrepancies in available measurements of the star's proper motion. Table 2 lists parallax and
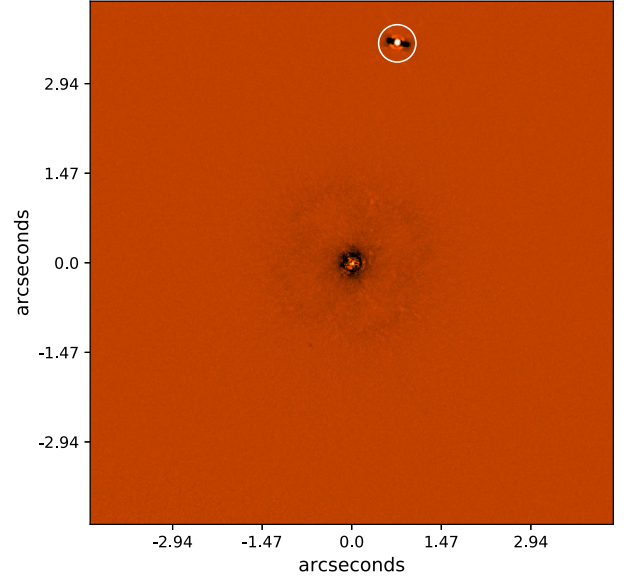
Figure 1. IRDIS K1-band PCA processed image of GJ 3346 from 2018 January 29th. The newly discovered companion GJ 3346 B is highlighted with a white circle.
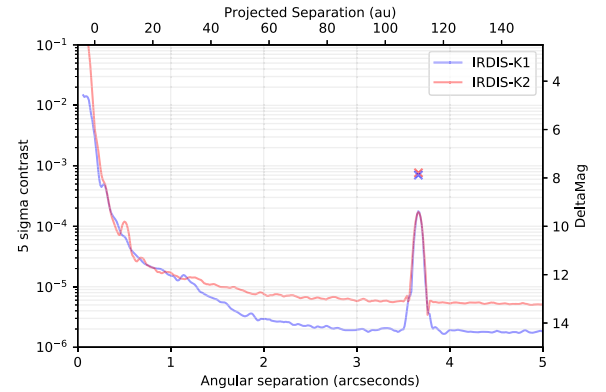
Figure 2. 5σ contrast limits achieved during the SPHERE observations of GJ 3346 in the two IRDIS filters. The position of GJ 3346 B is marked with a cross.

proper motion measurements found in major astrometric catalogues for GJ 3346. A total $\Delta\mu$ of 5.20 ± 1.84 mas yr^{-1} is obtained by comparing the Tycho-2 (Høg et al. 2000) and Tycho Gaia Astrometric Solution (TGAS; Michalik, Lindegren & Hobbs 2015) catalogues, as was done for our selection procedure with COPAINS (Fontanive et al. 2019b). A similar value is obtained using the values from the second Gaia Data Release (hereafter GDR2; Gaia Collaboration 2018) which was not available at the time of target selection, confirming its suitability as a survey target. In addition to the full five-parameter astrometric solution, including celestial position,

---

[1] www.eso.org/sci/facilities/paranal/instruments/sphere/inst/filters.html

Table 2. Stellar parameters of GJ 3346.

Parameter	Value	Reference
Age (Gyr)	4.3–6.5	This paper
M_{star} (M$_\odot$)	0.683 ± 0.018	This paper
R_{star} (R$_\odot$)	0.639 ± 0.014	This paper
V (mag)	8.72	*Hipparcos*
$B-V$ (mag)	1.003 ± 0.003	*Hipparcos*
$V-I$ (mag)	1.05	*Hipparcos*
G	8.3864 ± 0.0004	GDR2
$BP-RP$	$0.0640^{+0.0921}_{-0.0561}$	GDR2
J (mag)	6.856 ± 0.019	2MASS
H (mag)	6.284 ± 0.026	2MASS
K (mag)	6.205 ± 0.024	2MASS
RV (km s^{-1})	-14.02 ± 0.42	GDR2
U (km s^{-1})	-8.24 ± 0.35	This paper
V (km s^{-1})	11.13 ± 0.27	This paper
W (km s^{-1})	30.60 ± 0.23	This paper
ST	K3V	*Hipparcos*
T_{eff} (K)	4750 ± 65	This paper
$\log g$	4.50 ± 0.10	This paper
[Fe/H]	-0.38 ± 0.08	This paper
$v \sin i$ (km s^{-1})	3.5 ± 0.5	This paper
P_{rot}	13.0 ± 0.4	This paper
$\log R_{HK}$	-4.48	Wright et al. (2004)
$\log L_X/L_{bol}$	-4.89	This paper
EW Li (mÅ)	0.0	This paper
Parallax (mas)	41.09 ± 1.26	*Hipparcos*
	42.02 ± 0.28	TGAS
	42.0225 ± 0.0302	*Gaia* DR2
pmRA (mas yr^{-1})	174.3 ± 1.3	Tycho-2
	173.92 ± 0.87	*Hipparcos*
	174.023 ± 0.064	TGAS
	173.571 ± 0.046	*Gaia* DR2
pmDec (mas yr^{-1})	201.2 ± 1.3	Tycho-2
	204.52 ± 0.94	*Hipparcos*
	206.393 ± 0.064	TGAS
	207.558 ± 0.053	*Gaia* DR2

parallaxes, and proper motions, GDR2 also includes photometry in *Gaia*'s G, G_{BP}, and G_{RP} bands. Combining these information with all the available data from the literature, we were able to carefully reassess the values of stellar parameters for GJ 3346, which we report in Table 2, together with the photometry from *Gaia*, *Hipparcos* (Perryman et al. 1997), and 2MASS (Skrutskie et al. 2006).

3.1 Activity and rotation

The star is a K3 star which shows moderate chromospheric activity and X-ray emission. Wright et al. (2004) and Gray et al. (2006) measured $\log R_{HK} = -4.48$ and -4.45, respectively.[2] An X-ray luminosity of 1.01×10^{28} and $\log L_X/L_{bol} = -4.89$ were derived from *ROSAT* (Voges et al. 2000), following the procedures described in Desidera et al. (2015). The availability of TESS (Ricker et al. 2015) light curves for GJ 3346, shown in Fig. 3, also allowed us
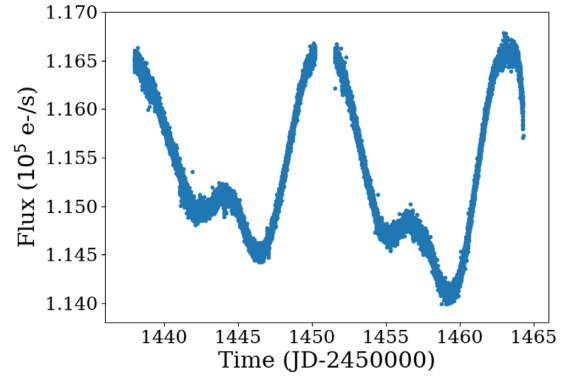
Figure 3. TESS light curve for GJ 3346.

to derive a photometric rotational period of 13.0 ± 0.4 d.[3] This is fully compatible with the observed magnetic and coronal activity.

3.2 Chemical abundances

A high-resolution spectrum (spectral coverage from 3800 to 10 000 Å with a resolution of $R = 57\,000$) of GJ 3346 obtained with FOCES (Pfeiffer et al. 1998) had been published by Maldonado et al. (2010), who claimed a marginal lithium detection, despite the high ($\sim$70) signal-to-noise ratio (SNR) per pixel at the position of the lithium 6708 Å line.

We used the same data (courtesy of J. Maldonado) to carry out spectroscopic parameter and abundance determination as done in our previous works (see e.g. D'Orazi et al. 2017, for line lists and solar abundances), by using MOOG by C. Sneden (1973, 2017 version) and the ODFNEW grids of model atmospheres (new opacities and no overshooting) by Castelli & Kurucz (2004). Atmospheric parameters were derived following the standard procedure: effective temperature (T_{eff}) and micro turbulent velocity (V_t) have been obtained by removing spurious trends between $\log n$(Fe I) and excitation potential and reduced equivalent widths (EWs) of the lines, respectively. The surface gravity ($\log g$) comes from the ionization equilibrium

$$\Delta[\log(\text{Fe I}) - \log(\text{Fe II})] < \sqrt{\sigma_1^2 + \sigma_2^2}, \tag{1}$$

where σ_1 and σ_2 are errors on the mean abundances from Fe I and Fe II, respectively.

We have derived $T_{eff} = 4750 \pm 65$ K, $\log g = 4.5 \pm 0.1$ dex, $V_t = 0.95 \pm 0.12$ km s^{-1}, and [Fe/H] $= -0.38 \pm 0.08$ (with the solar iron abundance being $\log n_\odot$(Fe I) $= 7.50$). We refer the reader to D'Orazi et al. (2017) for details on error budget computations. Our slightly metal-poor iron abundance is consistent with the finding of Mortier et al. (2013) ([Fe/H] $= -0.20$ from CORALIE and Gray et al. 2006, [M/H] $= -0.35$ from low-resolution spectroscopy). Abundances for the α elements Mg, Si, and Ca exhibit a marginal enhancement, suggesting a thin disc composition with [Mg/Fe] $= +0.10 \pm 0.12$, [Si/Fe] $= +0.07 \pm 0.09$, and [Ca/Fe] $= +0.19 \pm 0.11$ dex.

As a possible indication of pollution from the previous AGB companion we have also derived the s-process element Ba, to search

---

[2]The value of $\log R_{HK}$ from Wright et al. (2004) is derived from their tabulated S-Index value using the Noyes et al. (1984) prescriptions.

[3]Data obtained from https://mast.stsci.edu/portal/Mashup/Clients/Mast/Portal.html – TESS Obs ID: tess2018319095959-s0005-0000000442893646-0125-s.
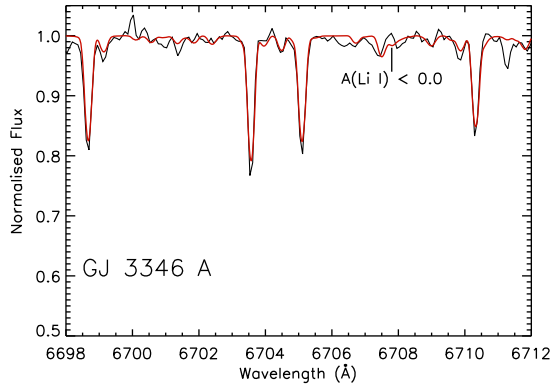
Figure 4. Spectral synthesis (red line) around the Li I line at 6707.8 Å for GJ 3346 A.

for enhancements. However, we did not detect any hint of overabundance with [Ba/Fe] = +0.05 ± 0.10 (see D'Orazi et al. 2017 and references therein for details on Ba abundance determination). The quality of the FOCES spectrum does not allow us to investigate in detail the occurrence of significant alterations of abundances other key elements, such as e.g. carbon, yttrium, zirconium, and lanthanum. However, the solar Ba abundance suggests that this is not the case and further investigations, by acquiring new high-quality (SNR ≳ 150), high-resolution spectra are not crucial in this context.

As shown in Fig. 4, a comparison between the observed and synthetic spectrum (calculated assuming $A(\text{Li}) = 0.00$) only allows to put an upper limit on the lithium abundances. We believe that the measurement reported by Maldonado et al. (2010) is likely a blended EW of the iron line. From the spectral synthesis including the Ba II (5853 Å) and Li spectral regions, we also derived the projected rotational velocity of the star ($v \sin i = 3.5 \pm 0.5 \, \text{km s}^{-1}$).

3.3 System age

GJ 3364 was originally classified as young based on the information on the rotation and chromospherical and coronal emission. Our revised values of these indicators, discussed in Section 3.1, are still compatible with an age of ∼ 600–700 Myr for GJ 3346. They could, however, also be explained assuming it is instead an older star rejuvenated by angular momentum accreted through stellar wind originated from the WD progenitor at the end of the AGB phase (see Zurlo et al. 2013, and references therein) or by tidal locking with a close stellar companion (see e.g. Hut 1981; Fleming et al. 2019).

The possibility of a tidally locked binary can easily be ruled out by the availability in the literature of several radial velocity (RV) measurements (Nordström et al. 2004; Maldonado et al. 2010; Gaia Collaboration et al. 2016a; Sperauskas et al. 2016; Riedel et al. 2017). These data show some scatter exceeding the formal errors (peak-to-valley differences of about 3 km s^{-1}) but the dispersion is low enough to exclude a tidally locked binary as source for the moderate magnetic activity of the star.

The lack of a clear lithium detection, on the other hand, also points towards an older age for the system, with the WD being responsible for the spin-up. This is not surprising considering that the projected separation of the WD (87 au) is similar to the one observed for HD8049 (50 au). HD 8049 is a system with a K-type central star, a WD companion and significant signature of rejuvenation (Zurlo et al. 2013). In the case of GJ 3346, the activity is significantly

lower than that of HD8049. We expect this is due to an earlier event of mass-loss from the WD progenitor and subsequent accretion. If this was the case, we would have expected a significantly longer cooling age for the WD around GJ 3346.

The relatively low metallicity discussed in Section 3.2 is another indication for an old age since nearby young stars typically have chemical composition close to solar (D'Orazi, Biazzo & Randich 2011; Biazzo et al. 2017), which is also supported by the stellar kinematics. While kinematic arguments do not provide a well-defined age (a part from the case of members of moving groups or associations with well-defined age), it can still be used to obtain robust limits. Using *Gaia* DR2 astrometric values and absolute RV we obtain U, V, $W = -8.24$, 11.12, 30.60 km s^{-1}. The W velocity is well outside the kinematic space of young stars (Montes et al. 2001) and U and V velocities are also marginally inconsistent with it. This confirms that the star is older than 1 Gyr.

We finally tried to derive the age of the system through isochrone fitting, using the PARAM[4] (da Silva et al. 2006) web interface and adopting spectroscopic T_{eff} and [Fe/H], GDR2 parallax, and V band magnitude. The resulting value of 5.3 ± 3.4 Gyr is inconclusive, as expected for a K dwarf close to the main sequence. The stellar mass resulting from this fit is of 0.683 ± 0.018 M$_\odot$.

Given the ambiguities described above, we decided to adopt a different approach and tried to assess the most probable system age by estimating the typical values for stars with kinematics and metallicity similar to those of GJ 3346. We selected from Casagrande et al. (2011), the stars with metallicity and Galactic orbit similar to GJ 3346 (eccentricity between 0.04 and 0.10; maximum height over the Galactic plane between 0.70 and 0.82, [Fe/H] between −0.2 and −0.6). All the objects with blended photometry were then removed, which yielded a sample of 13 objects (beside GJ 3346), none of which detected in X-ray or with reported signatures pointing towards an age lower than 1 Gyr in the literature. We finally derived the stellar ages for these targets using PARAM, adopting effective temperature and [Fe/H] from Casagrande et al. (2011), obtaining a median value of the age is 5.3 Gyr with a dispersion of 2.5 Gyr. The median values of minimum and maximum ages obtained using the error bars provided by the PARAM web interface are 4.3 and 6.5 Gyr, respectively. We chose to use these as the adopted age range of the system, as this is still consistent with the estimated isochrone age for GJ3346, but more accurate.

4 RESULTS

4.1 Detection of a comoving WD companion to GJ 3346

A point source at a separation of 3.665 ± 0.002 arcsec and a position angle of 348.31 ± 0.09 deg from GJ 3346 was retrieved in our IRDIS images (see Fig. 1). A source compatible with the candidate identified in the IRDIS field of view was also retrieved in *Gaia* DR2 ($\rho = 3.647 \pm 0.001$ arcsec, PA = 347.89 ± 0.02 deg, see Table 3 for details). The fact that the GDR2 parallax and proper motion of this object were very similar to those of GJ 3346 provided a strong indication of its comoving nature, despite the apparent discrepancies within the single values. In fact, as discussed in Fontanive et al. (2019a), differences in both parallax and proper motion such as the ones observed here are to be expected in kinematics measurements made over a short time span, as is the

[4]http://stev.oapd.inaf.it/cgi-bin/param_1.3

Table 3. Relative photometry and astrometry of GJ 3346 B.

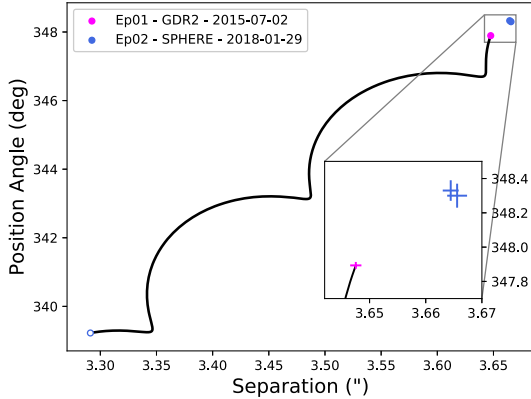| Epoch	Filter	λ_c (μm)	Contrast (Δmag)	Separation (mas)	PA (°)
2015.5	*Gaia G*	639.74	5.829 ± 0.005	3647.55 ± 1.00	347.8935 ± 0.02
	Gaia BP	516.47	4.228 ± 0.150		
	Gaia RP	783.05	4.686 ± 0.136		
2018.05	IRDIS *K*1	2.1025	7.844 ± 1.628	3665.59 ± 1.77	348.30 ± 0.07
	IRDIS *K*2	2.2550	7.788 ± 0.057	3664.45 ± 1.42	348.33 ± 0.06

Figure 5. Common proper motion analysis of GJ 3346 and its companion over the ∼2.5 yr baseline between GDR2 (magenta) and the astrometry from our SPHERE data (blue). The black line shows the motion of a background object relative to GJ 3346 based on the GDR2 parallax and proper motion of the primary over the same time frame, and the blue open circle indicates the expected position of a background object at the epoch of the SPHERE detection. The close companion is clearly found to be comoving with our target.

case for GDR2 parameters, which capture the reflex orbital motions in the components of multiple systems. Indeed, for $\Delta\mu$ binaries, short-term proper motions will by definition be deviant from the centre-of-mass motion of the pair, and in different directions for the two components at opposite ends of their orbits. In addition, the presence of the bright primary within few arcseconds almost certainly affected the quality of the *Gaia* DR2 five-parameter astrometric solution for GJ 3346 B, which appears to be relatively poor (its Renormalized Unit Weight Error[5] is in fact ∼4, as opposed to the typical value of 1.4 expected for a good fit.)

To further confirm the comoving nature of GJ 3346 B, we estimated the expected motion of a background star relative to GJ 3346 over the 2.5 yr baseline between our SPHERE observation and *Gaia* DR2, given the parallax and proper motion of the primary. The results, plotted in Fig. 5, clearly show that the measured positions (reported in Table 3) are incompatible with a background source, thus validating the idea that the pair is physically associated.

4.2 Companion photometric characterization

The values of the photometry of GJ 3346 B obtained from the IRDIS data using the VIP package (Gomez Gonzalez et al. 2017) and those retrieved from the Gaia DR2 catalogue are shown in Tables 3 and 4. While the red colour in the IRDIS bands pointed

---

[5]RUWE, described in detail in http://www.rssd.esa.int/doc_fetch.php?id = 3757412.

Table 4. Summary of the properties of GJ 3346 B.

Parameter	Value	Reference
Projected separation (au)	86.50 ± 0.06	This work
Current Mass ($M_\odot$)	0.58 ± 0.01	This work
IRDIS-*K*1 (mag)	14.04 ± 1.64	This work
IRDIS-*K*2 (mag)	13.99 ± 0.07	This work
Gaia G (mag)	14.22 ± 0.01	GDR2
Gaia BP (mag)	13.19 ± 0.15	GDR2
Gaia RP (mag)	12.59 ± 0.14	GDR2
Parallax (mas)	42.30 ± 0.07	GDR2
pmRA (mas yr^{-1})	182.24 ± 0.10	GDR2
pmDec (mas yr^{-1})	216.25 ± 0.12	GDR2
$T_{\rm eff}$ (K)	$11 \times 10^3 \pm 500$	This work
Cooling time (Myr)	684 ± 58	This work
Main-sequence time (Gyr)	$4.6^{+1.2}_{-1.0}$	This work
Original mass ($M_\odot$)	$1.20^{+0.10}_{-0.08}$	This work

towards a substellar nature for the companion, the photometry from *Gaia* lead us to think GJ 3346 B could be a WD instead. When we compared its colours with the ones of the objects in the WD locus from Hollands et al. (2018) (see Fig. 6), we found it to be compatible with the WD sequence considering the large colour error.[6] The blue colour of the companion is further supported by comparison of *Gaia* and SPHERE photometry, which yields *G-K*1 and *G-K*2 equal to 0.1266 and 0.2226, respectively. This is a further confirmation of the WD nature of GJ 3346 B. There is no available photometry in the UV from Galex, while *U*-band photometry of the whole system shows no or small UV excess, depending on the adopted *U*-band photometry (Mermilliod, Mermilliod & Hauck 1997; Koen et al. 2010), thus excluding a very hot source.

4.3 Derived physical parameters

As in Zurlo et al. (2013), we used a catalogue of empirical sequences using the catalogue of nearby WDs by Giammichele, Bergeron & Dufour (2012). The photometry values have been supplemented with available GALEX *FUV* and *NUV* magnitudes, and 2MASS *J*, *H*, and *K_S* magnitudes. The final sample consists of 107 nearby (≤51 pc) WDs: 22 with *FUV* magnitudes, 18 with *NUV* magnitudes, and 84 with *J*, *H*, *K_S* magnitudes calibrated by Giammichele et al. (2012). Along with the empirical catalogue we used the theoretical sequences of Vennes, Kawka & Németh (2011).

We calculated the effective temperature $T_{\rm eff}$ using the empirical

---

[6]The large *phot_bp_rp_excess_factor* (3.783) indicates a significant contamination by the primary on the *BP − RP* colour (Evans et al. 2018). The true colour is then likely bluer, better placing GJ 3346 B on the WD sequence.
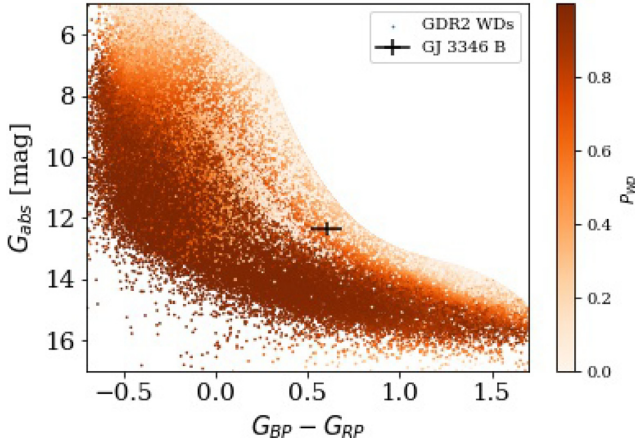
Figure 6. Position of GJ 3346 B (black square) in the GDR2 WD locus, as per the catalogue compiled by Gentile Fusillo et al. (2019). The colour scale indicates the probability of the source being a WD, $P_{\rm WD}$, as defined in the catalogue description.
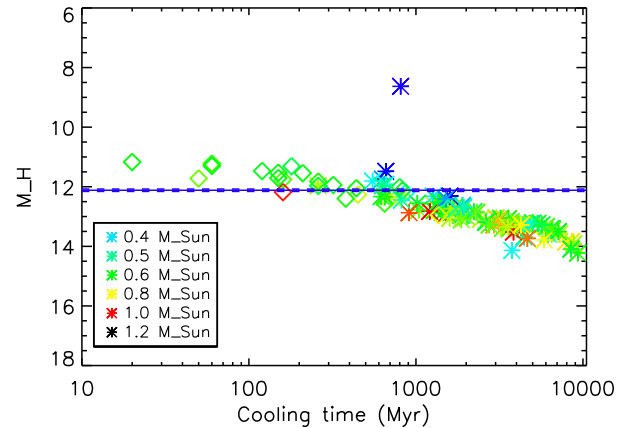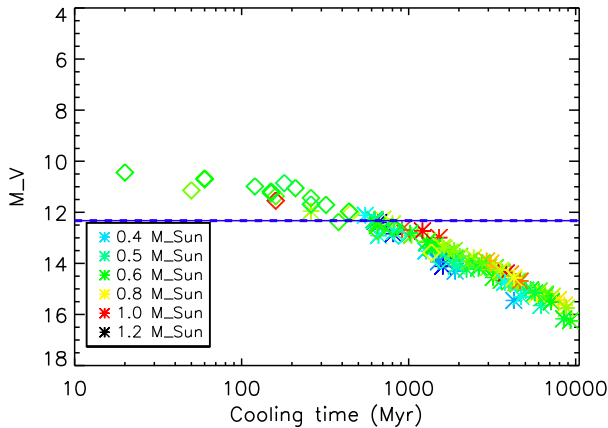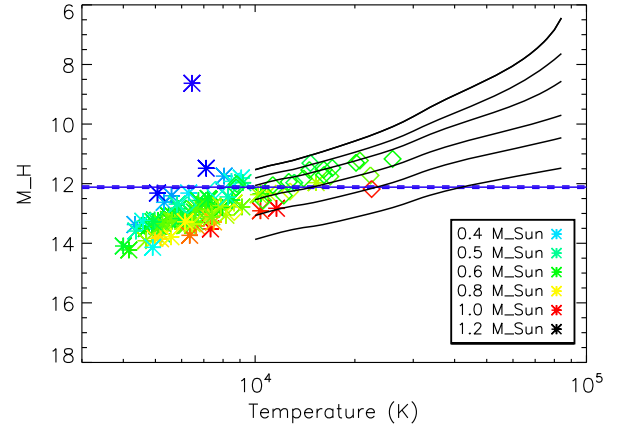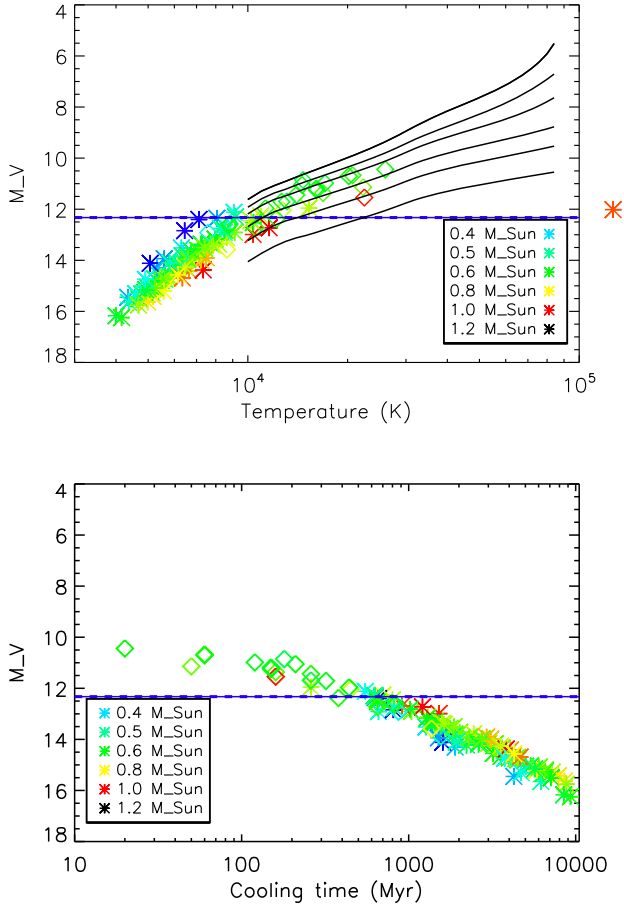
and theoretical sequences from the visible and NIR photometry of the WD. The result is a temperature of $\sim 11 \times 10^3$ K (see Fig. 7, top). This implies a value of the mass of the WD between 0.45 and 0.7 M$_\odot$. The cooling time calculated using the empirical sequences is 684 ± 58 Myr. (see Fig. 7, bottom).

4.4 System history

Coupling the estimates of the total system age and of the WD cooling time allows us some inferences of the most probable original configuration and evolution of the system. To this aim, we used the pre-WD lifetimes from the Bressan et al. (2012) models for the appropriate metallicity and the initial–final WD mass relationship by Cummings et al. (2018). Subtracting the WD cooling age from the system age yields a most probable pre-WD lifetime of 4.6 Gyr, with plausible limits between 3.6 and 5.8 Gyr. The corresponding initial masses are 1.20, 1.30, and 1.12 M$_\odot$, respectively, corresponding to WD masses of 0.585 ± 0.008 M$_\odot$ for the adopted relationship.

Neglecting the small amount of material accreted by the K-type component after the mass-loss and assuming adiabatic expansion of the orbit (Huang 1956; Boffin 2015), one could expect the original separation to have been roughly two thirds of the present one, i.e.
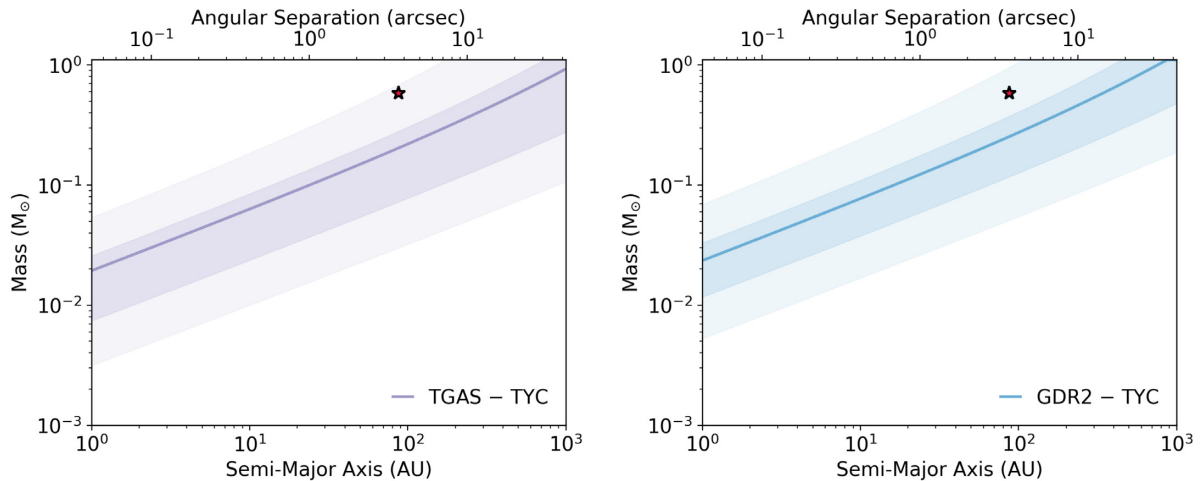

Figure 7. *Top.* Absolute magnitude in different bands (*V* and *H*) versus effective temperature for the WD models of Vennes et al. (2011) (black lines) and a sample of nearby dwarfs collected by Giammichele et al. (2012). Stars represent objects with all magnitudes available and diamonds represent the others. Colours indicate the mass from the lowest (blue) to the highest (red ones). The continuous blue horizontal line represents the magnitude of GJ 3346 B. The corresponding error bars are plotted as dashed blue lines. The plots show that the objects of the Giammichele et al. (2012) catalogue are not peculiar and are well described by the theoretical models of Vennes et al. (2011). *Bottom.* Absolute *V* and *H* magnitude versus cooling age of the WD.

Figure 8. Output of the COPAINS code for GJ 3346, showing predictions of the possible solutions for the mass and separation of the companion inducing the observed $\Delta\mu$ trend of the primary. The left-hand panel shows the expected position of the companion using a combination of the TGAS and Tycho-2 proper motions of the star, as used in the original target selection process, showing the median (solid line) and 1σ and 2σ intervals (dark and light shaded regions) of the possible solutions. The right-hand panel shows the same predictions made subsequently with GDR2 astrometry. The position of the detected WD companion is marked by the red star, compatible at the 1.5σ–2σ level with the expectations. We note however that the separation of the companion corresponds to a projected separation, while the dynamical predictions are in semimajor axis.

58 au. The true semimajor axis could be different due to orbit eccentricity and on-sky projection effects.

Younger/older system ages, corresponding to more/less massive WD progenitors, would imply a tighter/wider original configuration, respectively. While speculative, this evolution of the system would explain quite naturally all the observed features, including the rejuvenation of the K-type component through wind accretion (Jeffries & Stevens 1996).

4.5 Astrometric trend due to the WD companion

As previously noted, GJ 3346 has a strong $\Delta\mu$ offset between Tycho-2 and TGAS proper motions (Table 2). Assuming that the Tycho-2 measurement is close to the centre-of-mass motion of the system, and that *Gaia* provides a good approximation to the instantaneous velocity of the star, the COPAINS tool enables predictions of the possible masses and separations of the secondary companion. The analysis conducted with COPAINS on GJ 3346 revealed that the companion triggering the astrometric trend could be compatible with a substellar secondary on separations smaller than a few tens of au, or with a more massive stellar companion on a larger orbital distance. The results from the predictions made with COPAINS are shown in Fig. 8. The solid line shows the median set of solutions for the position of the bound companion, and the dark and light envelopes represent the 1σ and 2σ regions of confidence, respectively. The predictions assume a flat distribution in eccentricity and a face-on orbit.

As TGAS has a $\sim$25-yr baseline, this catalogue will only be a good estimate of short-term proper motions for systems with orbital periods on the century time-scale. As a result, the predictions made from TGAS measurements may not be accurate at small orbital separations (left-hand panel). None the less, the identified companion being on a wide orbit, this is not expected to affect our system. The position of the WD, indicated by the red star in Fig. 8, is indeed in agreement with the expectations from COPAINS within 2σ.

After the release of the *Gaia* DR2 catalogue, the same analysis was repeated with GDR2 for completeness and is shown in the right-hand panel. With a baseline of 22 months only, GDR2 truly captures

the reflex motion of the star under the gravitational influence of the WD, and provides an excellent approximation to an instantaneous velocity. The fact that the dynamical predictions in the two panels of Fig. 8 are very similar confirms that the time-scale of TGAS was also very short relative to the orbital period of the GJ 3346 AB system. The more accurate and better trusted COPAINS simulations made with GDR2 proper motions are consistent with the measured mass and observed separation of GJ 3346 B at the 1.5σ level.

5 DISCUSSION AND CONCLUSIONS

We detected a new WD companion around the K-type star GJ 3346, observed with SPHERE as part of the COPAINS pilot survey (Bonavita et al., in preparation) a program focused on young stars with significant proper motion difference between *Gaia* DR1 and Tycho-2. The companion was first detected in the SPHERE observations and then retrieved in *Gaia* DR2, which allowed to both confirm its comoving nature and to identify it as a WD companion.

Compared to similar systems discovered with similar methods (such as HD 8049, see Zurlo et al. 2013, for details), GJ 3346 lacked the abundance of information from the literature (in particular, there are no UV data), resulting in a less accurate estimate of the parameters of the WD and the possible original configuration of the system. We were none the less able to constrain its effective temperature ($11 \times 10^3 \pm 500$ K) and cooling age (684 ± 58 Myr).

The analysis of the central K star shows that the young age originally inferred from rotation and chromospheric and coronal emission is refuted by the lack of lithium, moderately low metallicity, and kinematics. The magnetic activity can be explained by spin-up of the star due to accretion of material and angular momentum at the end of the AGB phase of the WD component. Interestingly, the age from rotation and activity is close to the estimated cooling age of the WD, as found by Zurlo et al. (2013) for HD 8049 and by Leiner et al. (2018) for some other systems. This further supports the idea that accretion of angular momentum by the progenitor of the WD at the of the AGB phase reset the rotational clock of the star and then the rotational evolution proceeded as isolated stars after the accretion.

While the detection of the companion confirms the validity of our selection method, GJ3346 B is not suitable for a detailed analysis to obtain an estimate of its dynamical mass, as done for other objects showing significant $\Delta\mu$, such as HD 284149 B (Bonavita et al. 2017). Given its long period and the lack of information on its inclination and eccentricity,[7] such analysis, based on the method proposed by Makarov & Kaplan (2005) could only lead to a rather unreliable estimate of its minimum mass at best (Fontanive et al., in preparation, for a detailed description of the mass estimate method as well as its limitations).

With a projected separation of 87 au, GJ 3346 B is expected to cause an RV trend of $\sim$ 15–30 ms^{-1} yr^{-1} (estimated following the approach by Liu et al. 2002), which is well within reach of high-precision RV instruments, making it a promising case for detection. Further astrometric constraints on its mass will most likely also be provided by future *Gaia* releases. This discovery therefore confirms the key role played by *Gaia* in the discovery and characterization of faint companions, as well as the potential of dynamical pre-selection methods to enhance the yield of DI surveys.

ACKNOWLEDGEMENTS

REFERENCES

Amara A., Quanz S. P., 2012, MNRAS, 427, 948
Beuzit J. L. et al., 2019, A&A, 631, A155

---

[7]Given that the available RV was obtained with different instruments, it is not possible to obtain a reliable combination and to further constrain orbital parameters and minimum mass. Further observations at a precision of about 10 m s^{-1} spanning few years would be required to uncover a RV trend.

Biazzo K. et al., 2017, A&A, 605, A66
Boccaletti A. et al., 2008, in Hubin N., Max C. E., Wizinowich P. L., eds, Proc. SPIE Conf. Ser. Vol. 7015, Adaptive Optics Systems. SPIE, Bellingham, p. 70151B
Boffin H. M. J., 2015, in Boffin H. M. J., Carraro G., Beccari G., eds, Astrophysics and Space Science Library, Vol. 413, Ecology of Blue Straggler Stars. Springer-Verlag , Berlin, p. 153
Bonavita M. et al., 2017, A&A, 608, A106
Brandt T. D., 2018, ApJS, 239, 31
Bressan A., Marigo P., Girardi L., Salasnich B., Dal Cero C., Rubele S., Nanni A., 2012, MNRAS, 427, 127
Casagrande L., Schönrich R., Asplund M., Cassisi S., Ramírez I., Meléndez J., Bensby T., Feltzing S., 2011, A&A, 530, A138
Castelli F., Kurucz R. L., 2004, in Piskunov N., Weiss W. W., Gray D. F., eds, Modelling of Stellar Atmospheres, Poster Contributions, Proceedings of the 210th Symposium of the International Astronomical Union, IAU by the Astronomical Society of the Pacific, Uppsala, Sweden, p. A20
Chauvin G. et al., 2017, A&A, 605, L9
Claudi R. U. et al., 2008, in McLean I. S., Casali M. M., eds, Proc. SPIE Conf. Ser. Vol. 7014, Ground-based and Airborne Instrumentation for Astronomy II. SPIE, Bellingham, p. 70143E
Crepp J. R., Johnson J. A., Howard A. W., Marcy G. W., Gianninas A., Kilic M., Wright J. T., 2013, ApJ, 774, 1
Crepp J. R. et al., 2018, ApJ, 864, 42
Cummings J. D., Kalirai J. S., Tremblay P.-E., Ramirez-Ruiz E., Choi J., 2018, ApJ, 866, 21
D'Orazi V., Biazzo K., Randich S., 2011, A&A, 526, A103
D'Orazi V. et al., 2017, A&A, 598, A19
da Silva L. et al., 2006, A&A, 458, 609
Delorme P. et al., 2017, in Reylé C., Di Matteo P., Herpin F., Lagadec E., Lançon A., Meliani Z., Royer F., eds, SF2A-2017: Proceedings of the Annual meeting of the French Society of Astronomy and Astrophysics, Paris, p. 347
Desidera S., Barbieri M., 2007, A&A, 462, 345
Desidera S. et al., 2015, A&A, 573, A126
Desidera S., D'Orazi V., Lugaro M., 2016, A&A, 587, A46
Dohlen K. et al., 2008, in McLean I. S., Casali M. M., eds, Proc. SPIE Conf. Ser. Vol. 7014, Ground-based and Airborne Instrumentation for Astronomy II. SPIE, Bellingham, p. 70143L
Evans D. W. et al., 2018, A&A, 616, A4
Fleming D. P., Barnes R., Davenport J. R. A., Luger R., 2019, ApJ, 881, 88
Fontanive C., Rice K., Bonavita M., Lopez E., Mužić K., Biller B., 2019a, MNRAS, 485, 4967
Fontanive C., Mužić K., Bonavita M., Biller B., 2019b, MNRAS, 490, 1120
Fusco T. et al., 2006, in Ellerbroek B. L., Bonaccini Calia D., eds, Proc. SPIE Conf. Ser. Vol. 6272, Advances in Adaptive Optics II. SPIE, Bellingham, p. 62720K
Gaia Collaboration, 2016a, A&A, 595, A1
Gaia Collaboration, 2016b, A&A, 595, A2
Gaia Collaboration, 2018, A&A, 616, A1
Gentile Fusillo N. P. et al., 2019, MNRAS, 482, 4570
Giammichele N., Bergeron P., Dufour P., 2012, ApJS, 199, 29
Gomez Gonzalez C. A. et al., 2017, AJ, 154, 7
Gray R. O., Corbally C. J., Garrison R. F., McFadden M. T., Bubar E. J., McGahee C. E., O'Donoghue A. A., Knox E. R., 2006, AJ, 132, 161
Hadjidemetriou J. D., 1963, Icarus, 2, 440
Holberg J. B., Oswalt T. D., Sion E. M., Barstow M. A., Burleigh M. R., 2013, MNRAS, 435, 2077
Holberg J. B., Oswalt T. D., Sion E. M., McCook G. P., 2016, MNRAS, 462, 2295
Hollands M. A., Tremblay P.-E., Gänsicke B. T., Gentile-Fusillo N. P., Toonen S., 2018, MNRAS, 480, 3942
Huang S. S., 1956, AJ, 61, 49
Hugot E., Ferrari M., El Hadi K., Costille A., Dohlen K., Rabou P., Puget P., Beuzit J. L., 2012, A&A, 538, A139
Hurley J. R., Tout C. A., Pols O. R., 2002, MNRAS, 329, 897
Hut P., 1981, A&A, 99, 126
Høg E. et al., 2000, A&A, 355, L27

Iben Icko J., Livio M., 1993, PASP, 105, 1373

Jeffries R. D., Smalley B., 1996, A&A, 315, L19

Jeffries R. D., Stevens I. R., 1996, MNRAS, 279, 180

Koen C., Kilkenny D., van Wyk F., Marang F., 2010, MNRAS, 403, 1949

Langlois M. et al., 2012, in Ellerbroek B. L., Marchetti E., Véran J.-P., eds, Proc. SPIE Conf. Ser. Vol. 8447, Adaptive Optics Systems III. SPIE, Bellingham, p. 84473B

Leiner E., Mathieu R. D., Gosnell N. M., Sills A., 2018, ApJ, 869, L29

Liu M. C., Fischer D. A., Graham J. R., Lloyd J. P., Marcy G. W., Butler R. P., 2002, ApJ, 571, 519

Maire A.-L. et al., 2016, A&A, 587, A56

Makarov V. V., Kaplan G. H., 2005, AJ, 129, 2420

Maldonado J., Martínez-Arnáiz R. M., Eiroa C., Montes D., Montesinos B., 2010, A&A, 521, A12

Marois C., Lafrenière D., Doyon R., Macintosh B., Nadeau D., 2006, ApJ, 641, 556

Matthews C. T. et al., 2014, ApJ, 783, L25

McCrea W. H., 1964, MNRAS, 128, 147

Mermilliod J.-C., Mermilliod M., Hauck B., 1997, A&AS, 124, 349

Michalik D., Lindegren L., Hobbs D., 2015, A&A, 574, A115

Montes D., López-Santiago J., Gálvez M. C., Fernández-Figueroa M. J., De Castro E., Cornide M., 2001, MNRAS, 328, 45

Mortier A., Santos N. C., Sousa S., Israelian G., Mayor M., Udry S., 2013, A&A, 551, A112

Nordström B. et al., 2004, A&A, 418, 989

Noyes R. W., Hartmann L. W., Baliunas S. L., Duncan D. K., Vaughan A. H., 1984, ApJ, 279, 763

Pavlov A., Möller-Nilsson O., Feldt M., Henning T., Beuzit J.-L., Mouillet D., 2008, in Bridger A., Radziwill N. M., eds, Proc. SPIE Conf. Ser. Vol. 7019, Advanced Software and Control for Astronomy II. SPIE, Bellingham, p. 701939

Perryman M. A. C. et al., 1997, A&A, 500, 501

Petit C. et al., 2014, in Marchetti E., Close L. M., Véran J.-P., eds, Proc. SPIE Conf. Ser. Vol. 9148, Adaptive Optics Systems IV. SPIE, Bellingham, p. 91480O

Pfeiffer M. J., Frank C., Baumueller D., Fuhrmann K., Gehren T., 1998, A&AS, 130, 381

Ricker G. R. et al., 2015, J. Astron. Telesc. Instrum. Syst., 1, 014003

Riedel A. R., Alam M. K., Rice E. L., Cruz K. L., Henry T. J., 2017, ApJ, 840, 87

Sauvage J.-F. et al., 2010, in Ellerbroek B. L., Hart M., Hubin N., Wizinowich P. L., eds, Proc. SPIE Conf. Ser. Vol. 7736, Adaptive Optics Systems II. SPIE, Bellingham, p. 77360F

Schmid H. M. et al., 2018, A&A, 619, A9

Skrutskie M. F. et al., 2006, AJ, 131, 1163

Sneden C. A., 1973, PhD thesis, The University of Texas at Austin

Soummer R., 2005, ApJ, 618, L161

Soummer R., Pueyo L., Larkin J., 2012, ApJ, 755, L28

Sperauskas J., Bartašiūtė S., Boyle R. P., Deveikis V., Raudeliūnas S., Upgren A. R., 2016, A&A, 596, A116

Tokovinin A., Hartung M., Hayward T. L., Makarov V. V., 2012, AJ, 144, 7

Tokovinin A., Hartung M., Hayward T. L., 2013, AJ, 146, 8

Tremblay P. E. et al., 2017, MNRAS, 465, 2849

Vennes S., Kawka A., Németh P., 2011, MNRAS, 410, 2095

Vigan A., Moutou C., Langlois M., Allard F., Boccaletti A., Carbillet M., Mouillet D., Smith I., 2010, MNRAS, 407, 71

Vigan A. et al., 2017, A&A, 603, A3

Voges W. et al., 2000, A&A, 349, 389

Weidemann V., 2000, A&A, 363, 647

Wright J. T., Marcy G. W., Butler R. P., Vogt S. S., 2004, ApJS, 152, 261

Zurlo A. et al., 2013, A&A, 554, A21

This paper has been typeset from a TEX/LATEX file prepared by the author.